A Cascaded Controller for a Grid-tied Photovoltaic System with Three-phase Half-bridge Interleaved Buck Shunt Active Power Filter: Hybrid Control Strategy and Fuzzy Logic Approach

S. Echalih, A. Abouloifa, I. Lachkar, A. El Aroudi, Z. Hekss, F. Giri, M. Al-Numay

***Abstract*—This paper focuses on the control development of a grid-connected photovoltaic system coupled with a shunt active power filter. The considered power plant consists of a PV panel, a single-capacitor three-half bridge interleaved buck converter connected to a three-phase power grid and a nonlinear load. This study aims to accomplish simultaneously three objectives: i) to ensure a high compensation level of current harmonics and reactive power consumed by the nonlinear load in order to perform power factor correction at the grid side; ii) to extract the maximum power from the PV panel regardless the climatic conditions; iii) to regulate the dc bus capacitor voltage to its reference provided by the MPPT controller. To this end, a controller using a two-loop cascade strategy is designed. First, the inner loop is developed with the hybrid automaton approach to formulate the switching control signals with the aim of guaranteeing a unitary power factor. Second, the outer loop is designed using fuzzy logic control to ensure the regulation of the photovoltaic voltage, while the perturb and observe algorithm is employed to perform maximum power point tracking. Finally, the system with the developed control scheme is simulated using MATLAB/SimPowerSystems environment. The obtained results confirm that the proposed controller is able to achieve the previous objectives under varying environmental conditions.**

***Index Terms*—Hybrid control, Photovoltaic system, Half bridge interleaved buck (HBIB) converter, Shunt active power filter, Fuzzy logic controller.**

I. Introduction

In order to meet the rising worldwide electricity demands, solar panels are considered one of the most useful natural energy sources for power production due to their abundance, reduction in the cost of photovoltaic (PV) modules, and minimum impact on the environment [1].

Grid-connected PV systems have been developed at an exponential rate in order to inject power into the electrical grid using power converters. However, these power conversion systems are considered as nonlinear loads for the power grid, generate significant harmonics and reactive currents that interact with the grid impedance causing harmonic voltages and affecting all users connected to the same point of common coupling (PCC) [2]. In order to overcome these issues, using shunt active power filter (SAPF) has been considered the most suitable solution since it offers a higher capacity of filtering. Recently, SAPF-integrated PV systems have become a powerful mean to improve the power supply quality [3], [4]. In this context, two principal strategies can be identified. In the first one, a dc-dc converter is employed to track a maximum power from the PV panels and an SAPF is used to perform PFC. In the second one, the PV generator is coupled directly to the power grid via an SAPF in order to ensure both maximum power point tracking (MPPT) and power factor correction (PFC) by compensating harmonics and reactive power simultaneously [5].

Nevertheless, the previous structure has many drawbacks. The fact is that the main circuit of SAPF (voltage source inverter) encounters one of the most hazardous modes which is the shoot-through phenomenon [6]. This problem arises when both switches of the same leg are simultaneously turned ON, causing the flow of extremely high currents which would destroy the devices or would reduce circuit efficiency [7]. In power electronics devices, dead time control is generally added to the circuit so as to eliminate this phenomenon but it affects the pulse width, and hence, the harmonic compensation performance reduces. Therefore, the overall reliability of the system gets worse.

In the literature, different topologies have been suggested to solve all the aforementioned problems. The most interesting of them is the interleaved buck (IB) converter [8], [9], which has the advantage of being free from shoot-through issues, because the switches are no longer located on the same leg. As a result, by eliminating the dead time control, the reliability is significantly improved. Recently, many control strategies have been suggested for interleaved buck SAPF. In [10], a fuzzy logic (FLC) controller-based i_d-i_q method has been suggested for a three phase FBIB-SAPF. An ADALINE neural network

(Corresponding author: Salwa Echalih e-mail: salwa.echalih-etu@etu.univh2c.ma)

Salwa Echalih, Abdelmajid Abouloifa, Ibtissam Lachkar, and Zineb Hekss are with ESE Laboratory, ENSEM of Casablanca, Hassan II University of Casablanca, Casablanca 20103, Morocco (e-mail: abdelmajid.abouloifa@etu.univh2c.ma; ibtissam.lachkar@etu.univh2c.ma; hekss.zineb-etu@etu.univh2c.ma).

Fouad Giri is with Normandie Univ, Unicaen, ENSICAEN, LAC, 14000 Caen, France (e-mail: fouadgiri@yahoo.fr).

Mohammed Al-Numay with Electrical Engineering Department, King Saud University, Saudi Arabia (e-mail: alnumay@ksu.edu.sa).

Abdelali El Aroudi is with the Department of Electronics, Electrical Engineering and Automatic Control, Universitat Rovira i Virgili, 43007 Tarragona, Spain (e-mail: abdelali.elaroudi@urv.cat).

A. El Aroudi acknowledges the support of the Spanish *Ministerio de Ciencia e Innovación* under grant PID2020-120151RB-I00. A. El Aroudi and M. Al-Numay extend their appreciation to the International Scientific Partnership Program ISPP at King Saud University for funding this research work through ISPP#00102.

method for multilevel FBIB-SAPF has been discussed in [11]. In [12], an enhanced particle swarm optimization has been proposed for a three-phase HBIB-SAPF. In [8], a half-wave strategy with PI regulator has been suggested for a single phase HBIB-SAPF. In [13], a multidimensional sliding mode controller has been designed for a single phase FBIB-SAPF. A hybrid control strategy with PI regulator for single phase HBIB-SAPF has been presented in [9]. In the same vein, hybrid controller for three single phase HBIB-SAPF has been discussed in [14].

Some of the previous controllers have been designed based on the direct control strategy in which the generation of the reference current for SAPF involves complicated methods that leads to computing time delays and needs powerful calculation devices. Also, all the above-mentioned works have only considered the interleaved buck structure of SAPF without PV sources.

This paper is devoted to the control of an energy system consisting of HBIB-SAPF and a PV panel. The main contributions of the present paper are summarized below:

- The integration of the PV generator to a HBIB-SAPF for assuring power quality improvement and active power injection to the nonlinear load.
- Unlike some existing studies [4], [5] in which the controller was designed using an averaged model, the proposed current inner controller here is developed based on a hybrid automaton model in which the system switch among numerous working modes, each mode being defined by different dynamic equations, where the shifts are triggered by the completion of certain conditions based on the system properties. The voltage outer controller is designed using FLC combined with perturb and observe (PO) algorithm. The combined, FLC and PO MPPT algorithm solution turns out to be convenient for the achievement a good tracking precision.

The remainder of the paper is structured as follows: the description and mathematical modeling of the studied three-phase HBIB-SAPF are discussed in Section 2. The details about controller design are provided in Section 3. Numerical simulations for system are presented in Section 4 showing the effectiveness of the proposed controller. Finally, Section 5 provides some concluding remarks.

II. System Description and Modeling

Fig. 1 shows the circuit diagram of the grid-tied PV system with three phase HBIB-SAPF considered in this study. As can be seen in this figure, the system includes three main parts, namely:

1) Power grid represented by a three-phase sinusoidal supply voltage in series with their internal impedances each formed by a resistor and an inductor $(r_{gj}, L_{gj};\ j = a, b, c)$.
2) Nonlinear load constituting of a three-phase full-bridge rectifier in parallel with an R-L network.
3) Three-phase HBIB converter fed by a PV source and used as an SAPF. The proposed topology uses three single-phase dual buck power cells connected with a common dc link capacitor C_{pv}. Each power cell consists of two IGBTs, two diodes, and two coupling inductors $(L_{1j}, L_{2j}; j = a, b, c)$. These interfacing inductors serve to connect the HBIB-SAPF with the grid voltage at the PCC and to smooth the filter current.

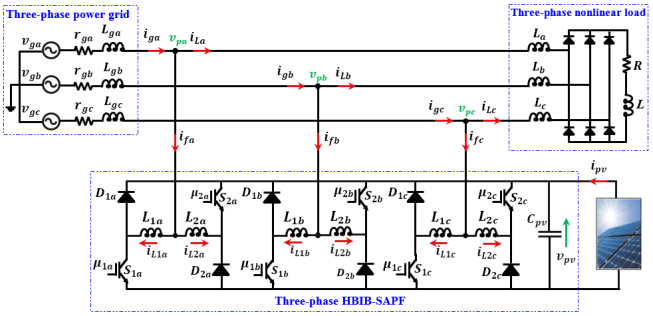

Fig. 1: Schematic circuit diagram of a grid-tied PV system with three-phase HBIB-SAPF.

The filter characteristics are significantly affected by the storage capacitance C_{pv}. In order to achieve good compensation performances, the parameters (C_{pv}, v_{pv}^*) should be selected according to the following:

- Dc-link voltage

In practice, the dc-link capacitor voltage must be over twice the grid voltage so as to ensure a proper current injection. The required minimum dc-link capacitor voltage $V_{pv,min}$ can be given as [15]:

$$V_{pv,min} \geq 2 \times V_g \tag{1}$$

where V_g is the peak value of the grid voltage.

- Dc-link capacitance

The optimum dc-link capacitance can be calculated as follows [16]:

$$C_{pv} = \frac{P_{pv}/V_{pv}}{2 \times \omega_g \times \Delta V_{pv}} \tag{2}$$

where P_{pv} is the power transferred by the PV panel at the MPP, V_{pv} is the dc-link voltage, ΔV_{pv} is the PV voltage ripple amplitude, and ω_g is the grid angular frequency.

The grid voltage is assumed to be sinusoidal, and it can be expressed as follows:

$$v_{gj}(t) = V_g \sin\left(\omega_g t - \frac{2\pi}{3}(i-1)\right); (j = a, b, c), (i = 1, 2, 3) \tag{3}$$

The resulting load currents $(i_{Lj}(t); j = a, b, c)$ can be expanded as Fourier series in steady-state operation as follow:

$$i_{Lj}(t) = \sum_{h=1}^{\infty} I_{j,h} \sin(h\omega_g t + \varphi_h); (j = a, b, c) \tag{4}$$

where $I_{j,h}$ and φ_h are, respectively, the amplitude and the phase of the h-th harmonic component of $i_{Lj}(t)$.

A. Three-phase HBIB-SAPF-PV modeling

1) Switched model: The IGBT-based HBIB converter operates according to the half-cycle modulation, where its significant feature is that the power switch works selectively depending on the direction of the output filter current i_{fj}. When i_{fj} is positive, (S_{1j}, D_{1j}) are the working pair, and when i_{fj} is negative (S_{2j}, D_{2j}) are another working pair. The binary switching signals of the HBIB converter $\{(\mu_{1j}, \mu_{2j})$; $j = a, b, c\}$ are defined by:

$$\mu_{1j} = \begin{cases} 1 & S_{1j} \text{ ON}; \quad D_{1j} \text{ OFF} \\ 0 & S_{1j} \text{ OFF}; \quad D_{1j} \text{ ON} \end{cases}$$
$$\mu_{2j} = \begin{cases} 1 & S_{2j} \text{ ON}; \quad D_{2j} \text{ OFF} \\ 0 & S_{2j} \text{ OFF}; \quad D_{2j} \text{ ON} \end{cases} \tag{5}$$

According to the polarity of the filter current, let us define the function μ_{3j} as follows:

$$\mu_{3j} = \begin{cases} +1 & \text{when} \quad i_{fj} > 0 \\ -1 & \text{when} \quad i_{fj} < 0 \end{cases} \quad (j = a, b, c) \tag{6}$$

By applying Kirchhoff's laws to the HBIB-SAPF-PV system, the switched model can be expressed as follows:

$$L\frac{di_{L1_j}}{dt} = \left(v_{p_j} + v_{pv_j}(2\mu_{1j} - 1)\right)\mu_{3j} \tag{7a}$$
$$L\frac{di_{L2_j}}{dt} = \left(v_{p_j} - v_{pv_j}(2\mu_{2j} - 1)\right)(1 - \mu_{3j}) \tag{7b}$$
$$C_{pv}\frac{dv_{pv}}{dt} = \left(i_{pv} - i_{L1_j}(2\mu_{1j} - 1)\right)\mu_{3j} + \left(i_{pv} + i_{L2_j}(2\mu_{2j} - 1)\right)(1 - \mu_{3j}) \tag{7c}$$

where i_{L1_j} and i_{L2_j} stand for the three-phase inductance currents, i_{pv} and v_{pv} are respectively the current and the voltage generated by the PV source and $\mu_{(1,2)j}$ are the driving signals for the switches (see Fig. 1). The parallel buck converters of each power cell are supposed identical which implies that $L_{1j} = L_{2j} = L$.

III. Controller design

The suggested controller is developed within two cascaded loops for achieving the control objectives. Its schematic block diagram is illustrated in Fig. 2.

A. Current inner loop design

To perform PFC, the current i_{gj} provided by the power grid must match the reference signal $i^*_{gj} = \beta v_{gj}$. This amounts to enforce the grid current to be proportional and in phase with the corresponding grid voltage v_{gj}. In fact, It can be noted that this can be carried out if the filter current i_{fj} injected by the HBIB-SAPF tracks, as closely as possible, the reference signal i^*_{fj} defined by the following expression:

$$i^*_{fj} = \beta v_{gj} - i_{Lj} \qquad (j = a, b, c) \tag{8}$$

where β is a suitable conductance setting the amplitude of the grid current.

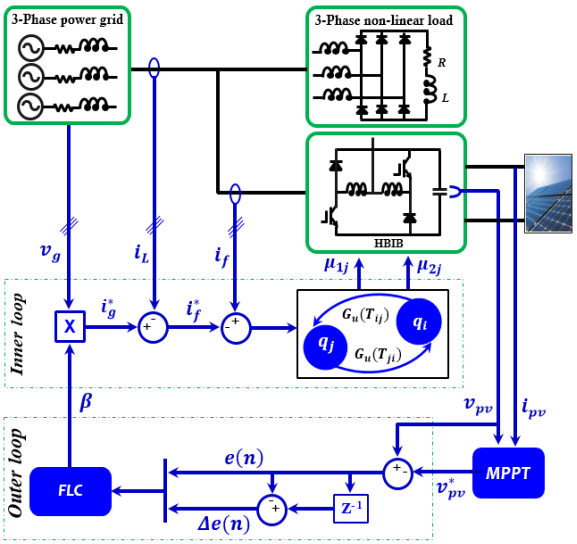

Fig. 2: Block diagram of the two-loop control system.

1) Hybrid automaton model: The instantaneous model developed above gives the exact evolution of the PV-fed HBIB-SAPF. It involves the interaction of discrete events and continuous-time dynamics described by differential equations. The hybrid automaton model of the PV-fed HBIB-SAPF converter is completely described by the following 6-tuple system [17]:

$$H = (Q, X, SC, T, G_u(T_{ij})) \tag{9}$$

According to the discrete states of the converter (μ_{1j}, μ_{2j}), one can discern, for each phase, four different discrete modes $Q = \{q_{1j}, q_{2j}, q_{3j}, q_{4j}\}$; $(j = a, b, c)$. $X = \mathbb{R}^3$ is the continuous state space which represents the operating states of the converter. f_g: $(Q \times X) \longrightarrow \mathbb{R}^3$ is the application that associates to each discrete mode a continuous-time model, and is defined by:

$$f_{qij} = \frac{dx_{ij}(t)}{dt} = A_{qij}X_j + B_{qij};\ (j = a, b, c), (i = 1, 2, 3, 4) \tag{10}$$

where $X_j = [x_1, x_2, x_3]^{\mathsf{T}}_j$, x_1 and x_2 represent the inductor currents (i_{L1} and i_{L2}), and x_3 represents the PV voltage v_{pv}. For the PV-fed HBIB-SAPF converter, each dual buck power cell can be represented in terms of four state equations, where each mode is related to a specific topology of the converter as shown in Fig. 3 and Table I. $T \subset Q \times Q$ represents the set of all possible transitions between discrete modes. $G_u(T_{ij})$ is the guard condition; it describes the constraint in the state space X to validate the transition from q_i to q_j.

2) Switching control law: To design a hybrid automaton for the studied system, the control problem reduces mainly to determining all possible transitions and their guard conditions $G_u(T_{ij})$ that will satisfy the regulation requirement of the system and at the same time will ensure the stability. According to the HBIB-SAPF converter properties presented in Table I and its operating characteristics provided in Remark 1, one can define the set of all possible transitions that occur from the q_i operating mode to q_j as follows

TABLE I: Model parameters according to (10).

Modes	Signals			Dynamics			Currents Evolution		
	μ_{1j}	μ_{2j}	μ_{3j}	A_j	B_j	$i_{fj}(t)$	$\frac{di_{L1j}}{dt}$	$\frac{di_{L2j}}{dt}$
q_{1j}	1	0	1	$\begin{bmatrix} 0 & 0 & \frac{1}{L} \\ 0 & 0 & 0 \\ \frac{-1}{C_{pv}} & 0 & 0 \end{bmatrix}$	$\begin{bmatrix} \frac{v_{pj}}{L} \\ 0 \\ \frac{i_{pv}}{C_{pv}} \end{bmatrix}$	>0	>0	0
q_{2j}	0	0	1	$\begin{bmatrix} 0 & 0 & \frac{-1}{L} \\ 0 & 0 & 0 \\ \frac{1}{C_{pv}} & 0 & 0 \end{bmatrix}$	$\begin{bmatrix} \frac{v_{pj}}{L} \\ 0 \\ \frac{i_{pv}}{C_{pv}} \end{bmatrix}$	>0	<0	0
q_{3j}	0	1	0	$\begin{bmatrix} 0 & 0 & 0 \\ 0 & 0 & \frac{-1}{L} \\ 0 & \frac{1}{C_{pv}} & 0 \end{bmatrix}$	$\begin{bmatrix} 0 \\ \frac{v_{pj}}{L} \\ \frac{i_{pv}}{C_{pv}} \end{bmatrix}$	<0	>0	0
q_{4j}	0	0	0	$\begin{bmatrix} 0 & 0 & 0 \\ 0 & 0 & \frac{1}{L} \\ \frac{-1}{C_{pv}} & 0 & 0 \end{bmatrix}$	$\begin{bmatrix} 0 \\ \frac{v_{pj}}{L} \\ \frac{i_{pv}}{C_{pv}} \end{bmatrix}$	<0	<0	0

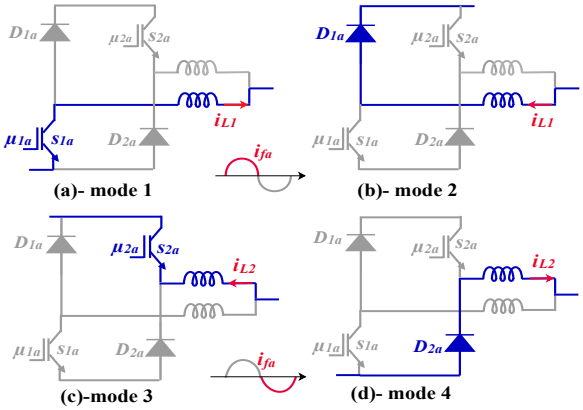

Fig. 3: Operation modes of HBIB converter in phase (a).

$\{T_{12}; T_{21}; T_{24}; T_{42}; T_{34}; T_{43}; T_{13}; T_{31}\}$.
The guard conditions of these transitions can be defined according to the dynamics of the filter current in the different functioning modes (see Table I) as follows:

At the positive half cycle ($i_{fj} > 0$), the set of transitions in this case 1 is ($T = T_{12}; T_{21}$) where their guard conditions $G_{uj}(T_{12})$ and $G_{uj}(T_{21})$ are given by:

$$\begin{cases} G_{uj}(T_{12}) = \{x \in X |\, i_{fj} > 0 \wedge (i_{fj} - i^*_{fj}) \geq +\varepsilon\} \\ G_{uj}(T_{21}) = \{x \in X |\, i_{fj} > 0 \wedge (i_{fj} - i^*_{fj}) \leq -\varepsilon\} \end{cases} \quad (11)$$

where ε are a suitable thresholds.

At the negative half cycle ($i_{fj} < 0$), the set of transitions in this case 2 is ($T = T_{34}; T_{43}$) where their guard conditions $G_{uj}(T_{34})$ and $G_{uj}(T_{43})$ are given by:

$$\begin{cases} G_{uj}(T_{34}) = \{x \in X |\, i_{fj} > 0 \wedge (i_{fj} - i^*_{fj}) \leq -\varepsilon\} \\ G_{uj}(T_{43}) = \{x \in X |\, i_{fj} > 0 \wedge (i_{fj} - i^*_{fj}) \geq +\varepsilon\} \end{cases} \quad (12)$$

Note that the threshold ε is used to make the switching less sensitive to noise and it is chosen as an infinitely small value.

On the other hand, the transition between the two cases (1 and 2) $\{T = T_{13}, T_{31}, T_{24}, T_{24}\}$, depend only on the filter current's direction in each phase. The corresponding guard conditions of these transitions are given as follows:

$$\begin{cases} G_{uj}(T_{13}) = \{x \in X |\, i_{fj} < 0\} \\ G_{uj}(T_{31}) = \{x \in X |\, i_{fj} > 0\} \\ G_{uj}(T_{24}) = \{x \in X |\, i_{fj} < 0\} \\ G_{uj}(T_{42}) = \{x \in X |\, i_{fj} > 0\} \end{cases} \quad (13)$$

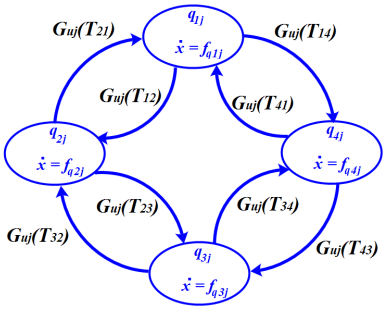

Fig. 4: State transition diagram for the proposed hybrid automaton controller of the PV-fed HBIB-SAPF converter.

Remark 1: Transition between modes is possible. However, from a functional point of view, there are certain restrictions that limit the number of admissible switches so as to guarantee the proper working of the entire system while achieving current tracking during its operation. Hence, based on the half-cycle operation of the interleaved buck converter, the filter current of each phase (a, b, c) is positive when the system transitions between modes q_1 and q_2. It becomes negative when it changes between modes q_3 and q_4.

Fig. 4 shows the state transition diagram for the proposed hybrid automaton controller of the PV-fed three-phase HBIB-SAPF converter. Each node stands for an operating mode represented by a system of differential equations. The arrows denote the discrete transitions: when a condition of transition is verified, the system switches to another mode.
The established transitions are given in order to ensure the adjustment of the filter current around the reference value and as a consequence, the compensation of harmonic and reactive currents generated by the non-linear load will be satisfactorily achieved.

B. PV generator reference voltage

In order to ensure that the PV array is operating at its proper maximum power point, an MPPT technique is required to generate a suitable reference, which will then be used by the outer loop for the dc-link voltage regulation. To this end, the P&O algorithm is used since it is easy to implement and needs fewer sensed variables. The main idea behind this algorithm is to periodically increment or decrement the output terminal voltage of the PV and comparing the power obtained in the current cycle to the one in past cycle. The basic steps of this algorithm can be seen in [18].

C. Voltage outer loop design

The main objective of the outer loop is to ensure the regulation of the dc-link voltage in order to maintain the power balance between the PV panel and the electrical power grid. To this end, the control signal β should be generated in such a way that the PV voltage v_{pv} be regulated to a reference signal v^*_{pv} provided by the MPPT generator. For achieving this regulation, an FLC is designed based on Mamdani inference [10]. Its schematic diagram is shown in Fig. 5, where it can be seen that the controller consists of two inputs, which are the

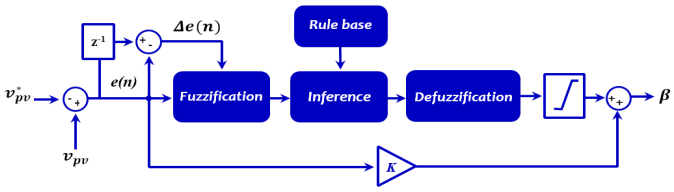

Fig. 5: Block diagram of the FLC.

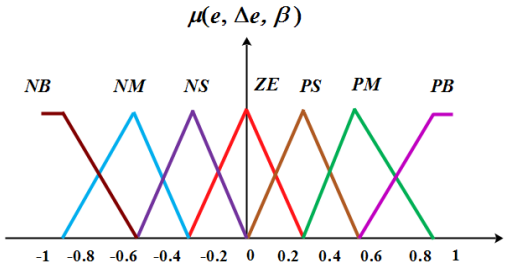

Fig. 6: Triangular membership functions of input and output variables.

error voltage $e(n) = v_{pv}(n) - v^*_{pv}(n)$ and the error difference $\Delta e(n) = e(n) - e(n-1)$ in n-th iteration, whereas the output is the control signal β. K is a corrective term, used to adjust this signal. The characteristics of the proposed FLC are:

- Seven fuzzy sets for each input and output: NB = Negative Big, NM = Negative Medium, NS = Negative Small, Z = Zero, PS = Positive Small, PM = Positive Medium, PB = Positive Big.
- Triangular membership functions are used for simplicity (Fig. 6).
- Fuzzification using continuous universe of discourse [10].
- Implication and aggregation using Mamdani's 'min' and 'max' operators.
- Defuzzification using the 'centroid' method [17].

The rule matrix for the dc voltage regulation are presented in Table II containing forty-nine rules. The elements of the rule table are obtained from an understanding of the HBIB-SAPF-PV behavior.

TABLE II: Control rules of the FLC.

	e						
Δe	*NB*	*NM*	*NS*	*ZE*	*PS*	*PM*	*PB*
NB	*NB*	*NB*	*NB*	*NB*	*NM*	*NS*	*ZE*
NM	*NB*	*NB*	*NB*	*NM*	*NS*	*ZE*	*PS*
NS	*NB*	*NB*	*NM*	*NS*	*ZE*	*PS*	*PM*
ZE	*NB*	*NM*	*NS*	*ZE*	*PS*	*PM*	*PB*
PS	*NM*	*NS*	*ZE*	*PS*	*PM*	*PB*	*PB*
PM	*NS*	*ZE*	*PS*	*PM*	*PB*	*PB*	*PB*
PB	*ZE*	*PS*	*PM*	*PB*	*PB*	*PB*	*PB*

IV. Simulation Results

The complete system including the designed controllers (Fig. 2) is simulated in Matlab/Simulink using SimPowerSystems environment and state flow toolbox. The ODE14x (Extrapolation) solver is selected with a fixed-step time of 1 µs. The switching frequency is 50 kHz. The detailed parameters

TABLE III: System parameters.

Subsystem	*Parameters*	*Values*
3-phase power grid	V_g	$230\sqrt{2}$ V
	f_g	50 Hz
	$r_{g(abc)}$, $L_{g(abc)}$	70 mΩ, 1 mH
Nonlinear load	R, L	15 Ω, 500 mH
	L_{abc}	3 mH
HBIB-SAPF	C_{pv}	6 mF
	L	3 mH

TABLE IV: PV electrical parameters of 1STH-225-P.

Parameter	**Symbol**	**Value**
Maximum power	P_m	213.15 W
Short circuit current	I_{sc}	7.84 A
Open circuit voltage	V_{oc}	36.9 V
Maximum power voltage	V_{mp}	29 V
Maximum power current	I_{mp}	7.35 A
Cell per module	N_{cell}	60
Parallel String	N_p	2
series-connected module	N_s	28

of the system and the PV panel are given in Tables III and IV. To test the performances of the closed-loop system, the following conditions are considered:

- Performance without PV panel.
- Performance with standard climatic conditions.
- Performance with solar irradiation variation.
- Performance with temperature variation.
- Comparison with other techniques.

The used nonlinear load consists of a three-phase full-bridge rectifier in parallel with an RL-network. It should be noticed that for all given operating scenarios, the load demands an average active power of 17.17 kW. The resulting load current i_{Labc} is illustrated in Fig. 7a. It is clearly visible that this current is actually rich in harmonic components being its THD of about 39.59%, as shown in Fig. 7b.

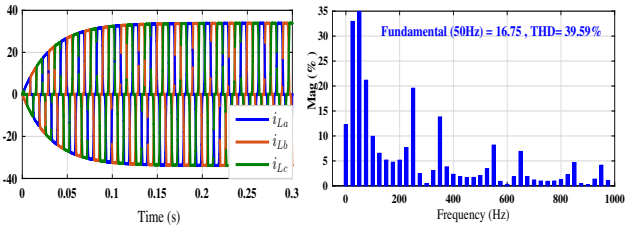

(a) (b)

Fig. 7: (a) Load current $i_{L_{abc}}$, (b) its harmonic content.

A. Performance without PV panel

In this case, the performance of the proposed controller is examined when the PV panel is disconnected. From the obtained results (Fig. 8), it can be seen that the system keeps working correctly only as a SAPF without PV system. However, the reference voltage across the capacitor C_{pv} is fixed at 800 V, instead of being generated by an MPPT control. Fig. 8a shows that the grid current is sinusoidal and in phase with the grid voltage, confirming that the compensation of harmonics and reactive power is well performed. In Fig. 8b, it

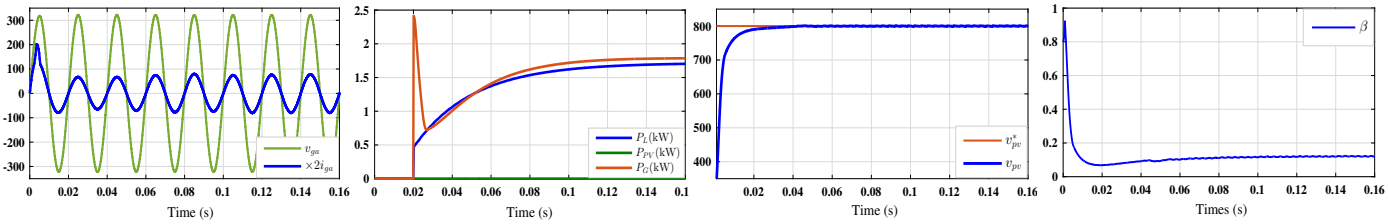

(a) Grid current i_{ga} and voltage v_{ga}. (b) P_{Load}, P_{PV}, and P_{Grid}. (c) PV voltage v_{pv} and its reference v_{pv}^*. (d) Control signal β.

Fig. 8: Controller performances without PV panel.

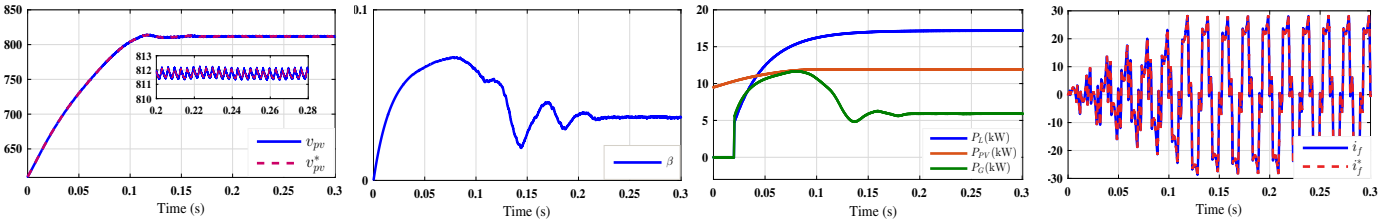

(a) v_{pv} and its reference v_{pv}^*. (b) Control signal β. (c) P_{Load}, P_{PV}, and P_{Grid}. (d) i_f and i_f^*.

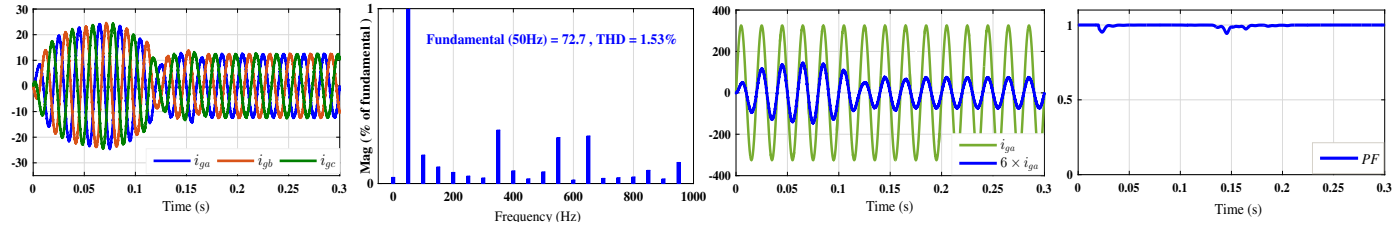

(e) Grid current i_{gabc}. (f) FFT spectrum of i_{gabc}. (g) Grid current i_g and voltage v_g. (h) Power factor.

Fig. 9: Controller performances with standard climatic conditions.

is clearly observed that the total power required by the load is provided only by the grid. Figs. 8c and 8d show respectively the dc-link voltage and the control signal β.

B. Performance with standard climatic conditions

The simulation results of the closed-loop system with PV panel under standard climatic conditions (T = 25 °C; G = $1\,\mathrm{kW/m^2}$) are shown in Fig. 9. Fig. 9a shows that the PV voltage tracks well its reference after a short transient period of $0.2\,\mathrm{s}$ and is kept regulated at $812\,\mathrm{V}$. Fig. 9b shows that the average of the signal β reaches its steady-state value after a short transient. In Fig. 9c, it is clearly seen that the power generated from the PV panel (P_{PV} = $11.93\,\mathrm{kW}$) supplies a part of the power required by the nonlinear load and residual load demand is served by the utility grid (P_{Grid}= $5.24\,\mathrm{kW}$). The filter current injected by the SAPF into the grid follows its reference with good precision, providing quick dynamic response and very good steady-state behavior of the hybrid automaton controller, as show in Fig. 9d. Indeed, it is observed in Fig. 9e that the resulting grid currents are sinusoidal with THD of about 1.53% (see Fig. 9g). This proves that the undesired harmonics are compensated for. Fig. 9g demonstrates that the PFC is well performed and the grid current and voltage are perfectly in phase. This is confirmed by a near unity value of power factor, as shown in Fig. 9h.

C. Performance with irradiation variation

In this case, the performance of the proposed controller is examined under the variation of solar irradiation whereas the temperature is kept constant ($T = 25°C$), as shown in Fig. 10a. More specifically, the irradiance G is decreased abruptly from $1\,\mathrm{kW/m^2}$ to $0.8\,\mathrm{kW/m^2}$ at time $0.35\,\mathrm{s}$ and is increased gradually from $0.8\,\mathrm{kW/m^2}$ to $0.9\,\mathrm{kW/m^2}$ at time $0.65\,\mathrm{s}$. It seen From Fig. 10 that the proposed nonlinear controller keeps the overall system in the optimal operating conditions with respect to irradiance variation. In fact, Fig 10b shows the perfect MPPT tracking in spite of irradiation changes. It is observed that the amount PV power is varied according to the solar irradiance variation (see Table V). The PV voltage follows well its desired reference after short transition periods, as shown in Fig. 10c. The evolution of the control signal β is illustrated in Fig. 10d. It shows that β reaches a new steady-state value after each irradiation change. It can be observed from Fig. 10e that the filter injected by HBIB-SAPF tracks well its reference with good precision. Furthermore, Fig. 10f shows that the grid current i_{gabc} remains its sinusoidal waveform at all instants. It is worth noting that the grid current's amplitude correlates with the irradiations' level. This current and the grid voltage are in phase despite the solar irradiance variation, as shown in 10g, proving thus the achievement of PFC. This is also demonstrated in Fig.10h

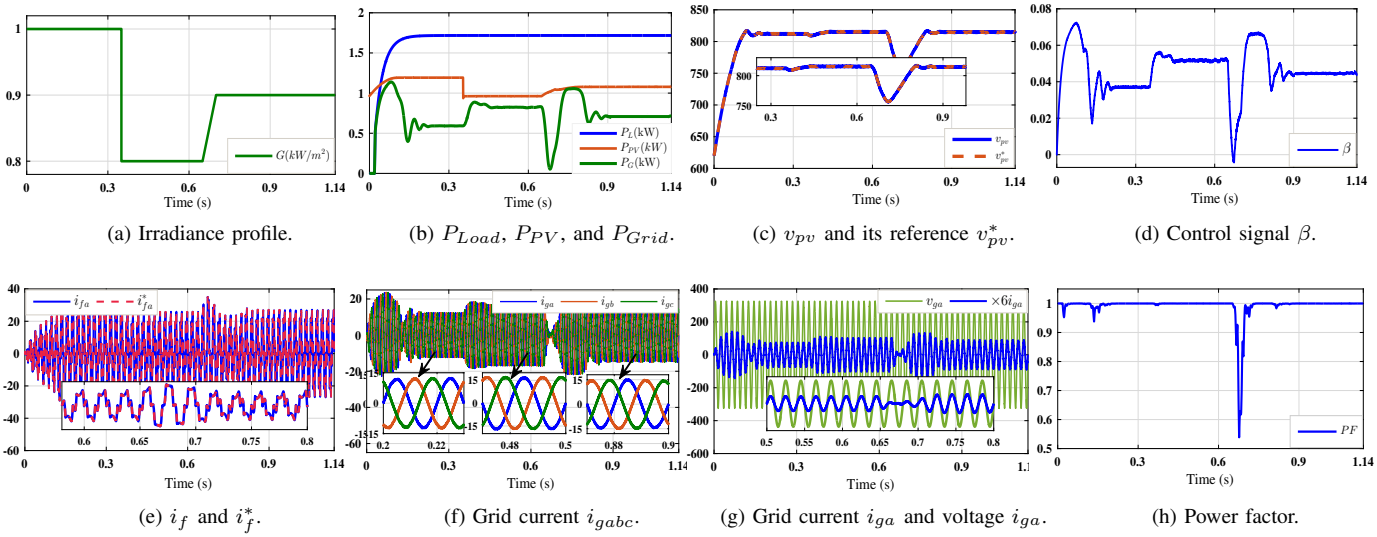

(a) Irradiance profile. (b) P_{Load}, P_{PV}, and P_{Grid}. (c) v_{pv} and its reference v^*_{pv}. (d) Control signal β.

(e) i_f and i^*_f. (f) Grid current i_{gabc}. (g) Grid current i_{ga} and voltage i_{ga}. (h) Power factor.

Fig. 10: Controller performances under solar irradiation variation.

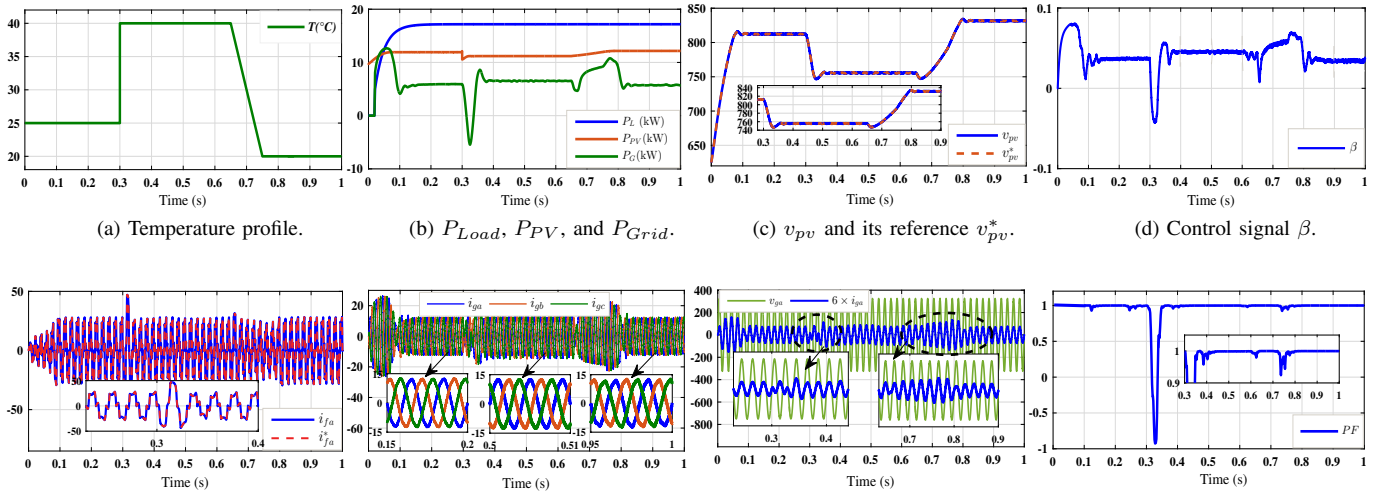

(a) Temperature profile. (b) P_{Load}, P_{PV}, and P_{Grid}. (c) v_{pv} and its reference v^*_{pv}. (d) Control signal β.

(e) i_f and i^*_f. (f) Grid current i_{gabc}. (g) Grid current i_{ga} and voltage v_{ga}. (h) Power factor

Fig. 11: Controller performances under temperature variation.

where the power factor is clearly close to 1.

D. Performance with temperature variation

In this case, the closed loop system is examined in presence of temperature variations as described in Fig. 11a. Namely, the temperature T is increased abruptly from $25\,^{\circ}\mathrm{C}$ to $40\,^{\circ}\mathrm{C}$ at $0.3\,\mathrm{s}$ and is decreased gradually from $40\,^{\circ}\mathrm{C}$ to $20\,^{\circ}\mathrm{C}$ at $0.65\,\mathrm{s}$, while the irradiation G is kept constant at $1\,\mathrm{kW/m^2}$. For the given operating scenario, one can see that, as expected, the temperature increase has a negative effect on the power generated by the PV panel (see Table V). When the temperature increases the PV power decreases and vice versa, as shown in Fig. 11b. Fig. 11c shows that the PV voltage reaches its desired reference value after a transient period. The evolution of the control signal β in front of the temperature variation is illustrated in Fig. 11d. Fig. 11e shows that the filter current injected by the HBIB-SAPF follows its reference with good accuracy. This guarantees that the grid current remain sinusoidal all the time, expect for a short transient period as shown in Fig. 11f. Fig. 11g shows that the grid current and voltage are in phase, which confirms that PFC is well performed. This is also demonstrated in Fig. 11h where a near unity power factor can be appreciated. The THD of the grid current under the change of climatic conditions are summarized in Table VI where it can be observed that the obtained THD values complies with the IEEE. std 519 which state that THD must be less than 5%.

E. Performance comparison with other techniques

Table VII shows a comparison between the proposed control technique and other methods in which some of criteria are considered such as Model, complexity, dependency on control

TABLE V: Maximum power points (MPP)

MPP	***G*** ($\mathrm{kW/m^2}$)	***T*** (°C)	***Max-power*** (kW)	***Max-voltage*** (V)
MPP1	1	25	11.93	812
MPP2	0.8	25	9.62	817.33
MPP3	0.9	25	10.77	810.98
MPP4	1	40	11.19	755.88
MPP5	1	20	12.16	830.96

TABLE VI: THDs of mitigated grid current.

Climatic conditions	**THD(%)**
	Before connecting SAPF-PV
	39.59%
	After connecting SAPF-PV
$G = 1000\,\mathrm{W/m^2}; T = 25\,^\circ\mathrm{C}$	1.53%
$G = 800\,\mathrm{W/m^2}; T = 25\,^\circ\mathrm{C}$	1.11%
$G = 900\,\mathrm{W/m^2}; T = 25\,^\circ\mathrm{C}$	1.35%
$G = 1000\,\mathrm{W/m^2}; T = 40\,^\circ\mathrm{C}$	1.63%
$G = 1000\,\mathrm{W/m^2}; T = 20\,^\circ\mathrm{C}$	1.98%

parameter, and THD. It is observed that the proposed method shows better performance in terms of THD value. Moreover, it shows less complexity than other methods since PWM or transformation blocks are not required.

TABLE VII: Comparison of performances between proposed and other methods.

Performance	*Sliding-mode* [5]	*Backstepping* [19]	*EPSO* [12]	Proposed
Model	Averaged	Averaged	Real	Hybrid
Complexity	High	High	Moderate	Simple
Control parameters dependency	Yes	Yes	blue Yes	No
PWM circuit	Yes	Yes	-	No
%THD of i_g	2.53-2.87%	2.35-2.90%	2%	<2%

V. Conclusion

The main focus of this paper is on study and control of the three-phase half-bridge interleaved buck converter operating as a shunt active power filter interfaced with a grid-tied photovoltaic system. In this study, a nonlinear controller based on the hybrid automaton approach and fuzzy logic control technique was developed to reach the desired control objectives including power factor correction, extraction of the maximum power from PV generator, as well as the regulation of dc voltage. According to the simulation results, it has been confirmed that the proposed controller is able to perform with good accuracy under various conditions.By using the hybrid automaton, the performances of the HBIB-SAPF have been improved achieving a power factor close to 1 and tolerable THD values ranging from 1.11% to 2.04%, hence complying with IEEE. std 519. On the other hand, the combined fuzzy logic regulator and PO MPPT algorithm successfully regulates the PV voltage to its desired reference, in both steady-state and changing weather conditions, ensuring the power transfer from the PV panels to the electrical power grid.

References

[1] Z. Hekss, A. Abouloifa, S. Echalih, and I. Lachkar, "Cascade nonlinear control of photovoltaic system connected to single phase half bridge shunt active power filter," in *2019 4th World Conference on Complex Systems (WCCS)*, April 2019, pp. 1–6.

[2] A. Abouloifa, F. Giri, I. Lachkar, F. Z. Chaoui, M. Kissaoui, and Y. Abouelmahjoub, "Cascade nonlinear control of shunt active power filters with average performance analysis," *Control Engineering Practice*, vol. 26, pp. 211–221, 2014.

[3] Z. Hekss, I. Lachkar, A. Abouloifa, S. Echalih, M. Aourir, and F. Giri, "Nonlinear control strategy of single phase half bridge shunt active power filter interfacing renewable energy source and grid," in *2019 American Control Conference (ACC)*, 2019, pp. 1972–1977.

[4] Z. Hekss, A. Abouloifa, J. Janik, I. Lachkar, S. Echalih, F. z. Chaoui, and F. Giri, "Hybrid automaton control of three phase reduced switch shunt active power filter connected photovoltaic system," *IFAC-PapersOnLine*, vol. 53, no. 2, pp. 12 847–12 852, 2020.

[5] Z. Hekss, A. Abouloifa, I. Lachkar, F. Giri, S. Echalih, and J. Guerrero, "Nonlinear adaptive control design with average performance analysis for photovoltaic system based on half bridge shunt active power filter," *Electrical Power and Energy Systems*, vol. 125, pp. 106–478, 2021.

[6] S. Abe, K. Hasegawa, M. Tsukuda, K. Wada, I. Omura, and T. Ninomiya, "Modelling of the shoot-through phenomenon introduced by the next generation IGBT in inverter applications," *Microelectronics Reliability*, vol. 76-77, pp. 465–469, 2017.

[7] R. Patel and A. K. Panda, "Real time implementation of pi and fuzzy logic controller based 3-phase 4-wire interleaved buck active power filter for mitigation of harmonics with id–iq control strategy," *International Journal of Electrical Power & Energy Systems*, vol. 59, pp. 66–78, 2014.

[8] S. Echalih, A. Abouloifa, Z. Hekss, and I. Lachkar, "Half wave control strategy of interleaved buck converter based single phase active power filter for power quality improvement," in *2019 4th World Conference on Complex Systems (WCCS)*, April 2019, pp. 1–6.

[9] S. Echalih, A. Abouloifa, Z. Lachkar, Ibtissamand Hekss, M. Aourir, and F. Giri, "Hybrid control of single phase shunt active power filter based on interleaved buck converter," in *2019 American Control Conference (ACC)*, July 2019, pp. 3636–3641.

[10] R. Patel, A. K. Panda, and A. Kumar, "Real-time analysis of fuzzy controlled 2C dual buck half-bridge shunt APF with different MFs for dynamic unbalanced load," in *2018 Technologies for Smart-City Energy Security and Power (ICSESP)*. Bhubaneswar: IEEE, Mar. 2018, pp. 1–6.

[11] S. R. Das, P. K. Ray, A. K. Sahoo, K. Balasubramanian, and G. S. Reddy, "Improvement of power quality in a three-phase system using an adaline-based multilevel inverter," *Frontiers in Energy Research*, vol. 8, p. 23, 2020.

[12] V. Gali, N. Gupta, and R. Gupta, "Experimental investigations on multitudinal sliding mode controller-based interleaved shunt APF to mitigate shoot-through and PQ problems under distorted supply voltage conditions," *International Transactions on Electrical Energy Systems*, vol. 29, no. 1, Jan. 2019.

[13] ——, "Enhanced particle swarm optimization based dc-link voltage control algorithm for interleaved sapf," *Journal of Engineering Science and Technology*, vol. 13, no. 10, pp. 3393–3418, 2018.

[14] S. Echalih, A. Abouloifa, J. Janik, I. Lachkar, Z. Hekss, F. z. Chaoui, and F. Giri, "Hybrid controller with fuzzy logic technique for three phase half bridge interleaved buck shunt active power filter," *IFAC-PapersOnLine*, vol. 53, no. 2, pp. 13 418–13 423, 2020.

[15] C. A. Quinn and N. Mohan, "Active filtering of harmonic currents in three-phase, four-wire systems with three-phase and single-phase non-linear loads," *Conference Proceedings - IEEE Applied Power Electronics Conference and Exposition - APEC*, pp. 829–836, 1992.

[16] N. Patel, N. Gupta, and R. C. Bansal, "Combined active power sharing and grid current distortion enhancement-based approach for grid-connected multifunctional photovoltaic inverter," *International Transactions on Electrical Energy Systems*, vol. 30, no. 3, mar 2020.

[17] S. Echalih, A. Abouloifa, I. Lachkar, J. M. Guerrero, Z. Hekss, and F. Giri, "Hybrid automaton-fuzzy control of single phase dual buck half bridge shunt active power filter for shoot through elimination and power quality improvement," *International Journal of Electrical Power & Energy Systems*, vol. 131, p. 106986, 2021.

[18] K. Ishaque, Z. Salam, and G. Lauss, "The performance of perturb and observe and incremental conductance maximum power point tracking method under dynamic weather conditions," *Applied Energy*, vol. 119, pp. 228–236, 2014.

[19] Z. Hekss, A. Abouloifa, I. Lachkar, A. El Aroudi, S. Echalih, M. Al-Numay, and F. Giri, "Advanced nonlinear controller of single-phase shunt active power filter interfacing solar photovoltaic source and electrical power grid," *International Transactions on Electrical Energy Systems*, p. e13237.

Salwa Echalih received her master's degree in data processing from the Faculty of Sciences Ben M'sick, Hassan II University of Casablanca, Morocco, in 2017. Currently, she is preparing her Ph.D. in the field of automatic control, renewable energies and power electronics at National School of Electricity and Mechanics (ENSEM), Hassan II University of Casablanca. Her research interests include power quality improvement of electrical energy, renewable energy systems, nonlinear control techniques, and hybrid control of active power filter based on interleaved buck converter.

Abdelmajid Abouloifa received his Ph.D. in control engineering from the University of Caen Basse-Normandie, Caen, France in 2008. He is currently Professor at National School of Electricity and Mechanics (ENSEM), Hassan II University of Casablanca. His main research areas include modeling, nonlinear control, observation of FACTS systems, actives filters, uninterruptible power supplies, and photovoltaic systems.

Ibtissam Lachkar received the graduate degree from the Normal High School of Technical Education, Rabat, Morocco, in 1995 and her degree of high depth studies from the Mohammedia School of Engineers, Rabat, in 2005. She received her Ph.D. from Mohammedia School of Engineers. Currently, she is a Professor at National School of Electricity and Mechanics (ENSEM), Hassan II University of Casablanca. Her research interests include modeling, nonlinear control, uninterruptible power supplies, and photovoltaic systems.

Abdelali El Aroudi (Senior Member, IEEE) received the Graduate degree in physical science from the Faculté des sciences, Université Abdelmalek Essaadi, Tetouan, Morocco, in 1995, and the Ph.D. degree (Hons.) in applied physical science from the Universitat Politècnica de Catalunya, Barcelona, Spain, in 2000. From 1999 to 2001, he was a Visiting Professor with the Department of Electronics, Electrical Engineering and Automatic Control, Technical School of Engineering, Universitat Rovira i Virgili (URV), Tarragona, Spain, where he became an Associate Professor in 2001 and a full-time tenure Associate Professor in 2005. His research interests include the field of structure and control of power conditioning systems for autonomous systems, power factor correction, renewable energy applications, stability problems, nonlinear phenomena, and bifurcations control. He is/was a Guest Editor of the IEEE Journal on Emerging and Selected Topics in Circuits and Systems Special Issue on Design of Energy-Efficient Distributed Power Generation Systems in 2015, a Guest Editor of the IEEE Transactions on Circuits and Systems– II: Express Briefs in 2018, a Guest Editor of Energies in 2018 and 2019, an Associate Editor of Electronics Letters from 2017 to 2020, and IET Circuits, Devices & Systems in 2018 and 2019 and the Associate Editor-in-Chief for IEEE Open Journal of Circuits and Systems from 2020 to 2021. He currently serves as an Associate Editor for International Journal of Circuit Theory and Applications and IET Power Electronics, and a Topic Editor in Energies.

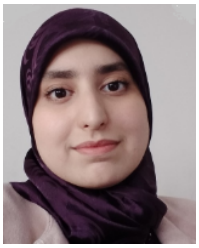

Zineb Hekss received her master's degree in data processing from the Faculty of Sciences Ben M'sick, Hassan II University of Casablanca, Morocco, in 2017. Currently, she is preparing her Ph.D. in the field of automatic control, renewable energies and power electronics at National School of Electricity and Mechanics (ENSEM), Hassan II University of Casablanca. Her research interests include renewable energy systems, power quality improvement of electrical energy, modeling, observation and nonlinear control techniques of active power filter associated with a photovoltaic system.

Fouad Giri Fouad Giri received the Ph.D. degree in automatic control from Institut National Polytechnique de Grenoble, France, in 1988. He is currently Professor at the University de Caen Normandie, France. His research interests include nonlinear system identification, observation and control for finite- and infinite-dimensional systems and application to power electric systems. He has published 6 books and over 120 journal papers. He has served as a Chair of the IFAC TC1.2 and Associate Editor for several journals including Automatica, Control Engineering Practice, IEEE Transactions on Control Systems Technology.

Mohammed S. Al-Numay (Member, IEEE) was born in Riyadh, Saudi Arabia. He received the B.S. degree (Hons.) in electrical engineering from King Saud University, Riyadh, in 1986, the M.S. degree in electrical engineering from Michigan State University, East Lansing, MI, USA, in 1990, and the Ph.D. degree in electrical engineering from the Georgia Institute of Technology, Atlanta, GA, USA, in 1997. Since 1998, he has been with the Electrical Engineering Department, King Saud University, where he is currently a Full Professor. From 2002 to 2006, he was the Dean of Admissions and Registration, King Saud University. Since 2008, he has been a Senior Consultant of Student Information Systems (SIS) and electronic admission to many governmental and private universities and colleges. He was appointed as the Assistant Vice Rector for Information Technology from 2015 to 2017. In January 2018, he became the Vice President of Educational and Academic Affairs, King Saud University. His research interests include modeling and control of switched mode power supplies and modeling and control of switched mode power supplies.